Photonuclear reactions on stable isotopes of selenium at bremsstrahlung end-point energies of 10−23 MeV

F.A. Rasulova[1,2†] N.V. Aksenov[1] S.I. Alekseev[1] R.A. Aliev[3,4] S.S. Belyshev[5,6] I. Chuprakov[1,7] N.Yu. Fursova[5,6] A.S. Madumarov[1] J.H. Khushvaktov[1,2] A.A. Kuznetsov[5,6] B.S. Yuldashev[1,2]

[1]Joint Institute for Nuclear Research, Dubna, Russia
[2]Institute of Nuclear Physics of the Academy of Sciences of the Republic of Uzbekistan, Tashkent, Uzbekistan
[3]Faculty of Chemistry of Lomonosov Moscow State University, Moscow, Russia
[4]National Research Center "Kurchatov Institute", Moscow, Russia
[5]Skobeltsyn Institute of Nuclear Physics of Lomonosov Moscow State University, Moscow, Russia
[6]Faculty of Physics of Lomonosov Moscow State University, Moscow, Russia
[7]Institute of Nuclear Physics, Almaty, Republic of Kazakhstan

Abstract: In this study, experiments were performed at bremsstrahlung end-point energies of 10−23 MeV with the beam from the MT-25 microtron using the γ-activation technique. The experimental values of relative yields were compared with theoretical results obtained on the basis of TALYS with the standard parameters and the combined model of photonucleon reactions. Including isospin splitting in the combined model of photonucleon reactions allows describing experimental data on reactions with proton escape in the energy range from 10 to 23 MeV. Therefore, taking into account isospin splitting is necessary for a correct description of the decay of the giant dipole resonance.

Keywords: bremsstrahlung photon, cross section, isospin splitting, giant dipole resonance

DOI: 10.1088/1674-1137/ad11e4

I. INTRODUCTION

Photonuclear reactions play an important role in basic and applied nuclear physics research [1−4]. The development of both nuclear physics research and applications based on photonuclear reactions is closely related to the development of attendant photon sources and measuring instruments. Photoneutron reactions on isotopes of a natural mixture of selenium have been well studied using bremsstrahlung γ-radiation [5−14], positron annihilation in flight [15], and Compton backscattering of laser beam photons [16−20]. Cross sections of photonuclear reactions on selenium isotopes in the region of giant dipole resonance (GDR) energy have been measured in several studies. In [5], on bremsstrahlung, the cross section for reactions $\sigma(\gamma, n)$ on all isotopes of natural selenium were measured up to an energy of 25 MeV. In [6], the same method was used to measure the cross sections for the reactions ^{78}Se(γ, n)^{77m}Se, ^{80}Se(γ, n)^{79m}Se, and ^{82}Se(γ, n)^{81m}Se. In [16−20], on a beam of quasi-monoenergetic photons obtained as a result of Compton backscattering, the cross sections for reactions $\sigma(\gamma, n)$ were measured in the energy range from the threshold to 14.6 MeV on ^{76,77,78,80}Se isotopes. In [15], on a beam of quasi-monoenergetic photons, the reaction cross section $\sigma(\gamma, 2n)$ and the sum of the reaction cross sections $\sigma(\gamma, n) + \sigma(\gamma, 1n1p)$ were measured in the energy range from the threshold to 30 MeV on ^{76,78,80,82}Se isotopes.

Experimental data on the cross sections of photoproton reactions on selenium isotopes are not available in the literature. With the exception of our previous works [13, 14], wherein multiparticle reactions on natural selenium were studied using end-point energies ranging from 20 to 80 MeV, all other previous studies investigated only photoneutron reactions on the stable isotopes of selenium. Thus, to obtain more information regarding reactions with a higher degree of complexity, this study investigated photonucleon emission reactions on natural selenium target nuclei, expressed as ^{nat}Se(γ, 1n) and ^{nat}Se(γ, 1p), using bremsstrahlung end-point energies of 10 to 23 MeV.

Photonuclear reactions are the main mechanism behind the formation of bypassed nuclei in the process of nucleosynthesis. The abundance of the lightest p-nucleus ^{74}Se can be described satisfactorily [21]. One of the aims of this work was to measure the relative yields of reactions on mixtures of natural isotopes of selenium that result in the formation and decay of ^{74}Se. The experiment-

Received 2 September 2023; Accepted 4 December 2023; Published online 5 December 2023

† E-mail: rasulova@jinr.ru

©2024 Chinese Physical Society and the Institute of High Energy Physics of the Chinese Academy of Sciences and the Institute of Modern Physics of the Chinese Academy of Sciences and IOP Publishing Ltd

ally obtained results were compared with the results of calculations based on TALYS-1.96 [22] with the standart parameters and the combined model of photonucleon reactions (CMPR) [23]. In addition, photoproton reaction products are potential medical isotopes, namely, ^{76}As [24] and ^{77}As [25, 26]; this means that studying the reaction cross sections is useful for both research and application purposes.

II. EXPERIMENTAL SET-UP AND PROCEDURES

This work was performed with the output electron beam of the MT-25 microtron [27]. The electron energies were in range of 10−23 MeV with an energy step of 1 MeV. To produce gamma radiation, a radiator target made of tungsten, which is a common convertor material, was used. The tungsten target was sufficiently thick (3 mm) to maximize the number of photons in the energy range of the GDR that dominates the photonuclear cross section from the nucleon separation threshold to 20–30 MeV. To remove the remaining electrons from the bremsstrahlung beam, a 30 mm thick aluminum absorber was placed behind the tungsten converter [28]. The target of natural selenium was at a distance of 1 cm from the converter.

In the experiments, natural selenium samples in metallic form were irradiated with a flux of bremsstrahlung, which was formed in the tungsten converter. The changes in beam current were measured using a calibrated ionization chamber in the beam and a Faraday cup and recorded in a web-accessible database for use during the analysis employing an analog-to-digital converter card and LabView software. In addition to the ionization chamber and Faraday cup, the electrical charge collected on the target was digitized and used to measure the beam current. The main parameters of the experiments are listed in Table 1. After irradiation, when the radiation levels in the experimental hall became safe, the targets were transferred to a separate measuring room, where the induced activity in the irradiated target was measured. We used a high purity germanium (HPGe) γ-detector with resolution of 16 keV at 1332 keV in combination with standard measurement electronics and a 16K ADC/MCA (Multiport II Multichannel Analyzer, CANBERRA). The energy and efficiency calibrations of the HPGe detector were carried out using standard gamma-ray sources. The procedure for gamma-activation measurements used in this work is described in detail in [28−30].

The time from the end of irradiation to the start of measurement (cooling time) was in range from 10 to 15 min. For each sample, the spectra were measured at several times during an overall period of 0.5, 1, 2, 6, 12, and 24 h. Typical γ-ray spectra of the reaction products produced from the ^{nat}Se are shown in Fig. 1. The sample was irradiated with bremsstrahlung radiation with end-point energy of 23 MeV.

The gamma-ray spectra were processed using the DEIMOS32 code [31], which fits the count area of the full-energy peaks with the Gaussian function. The identification of the processed peaks was based on the gamma-ray energy and intensity and the half-life of the generated residual nuclei. The radionuclides produced were identified based on their characteristic γ-ray energies and half-lives. The main γ-ray energies and intensities used to determine the yield of the reaction products are listed in

Table 1. Main parameters of the experiments.

Energy of electrons/MeV	Mass of selenium target/mg	Electron beam pulse current/μA	Integral number of electrons incident on the tungsten converter ($\times 10^{16}$)	Irradiation time/min
10	722.66	19	42.75 ± 4.28	60
11	693.02	10	45.0 ± 4.5	120
12	707.09	10.5	47.25 ± 4.72	120
13	741.20	10	22.5 ± 2.25	60
14	682.06	10	11.25 ± 1.12	30
15	712.51	10	4.875 ± 0.487	13
16	702.77	10	1.875 ± 0.187	5
17	233.48	5	1.875 ± 0.187	10
18	117.83	5	1.875 ± 0.187	10
19	89.26	5	1.875 ± 0.187	10
20	78.35	3	2.25 ± 0.225	20
21	78.36	3	2.25 ± 0.225	20
22	73.48	5	1.875 ± 0.187	10
23	70.22	5	1.875 ± 0.187	10

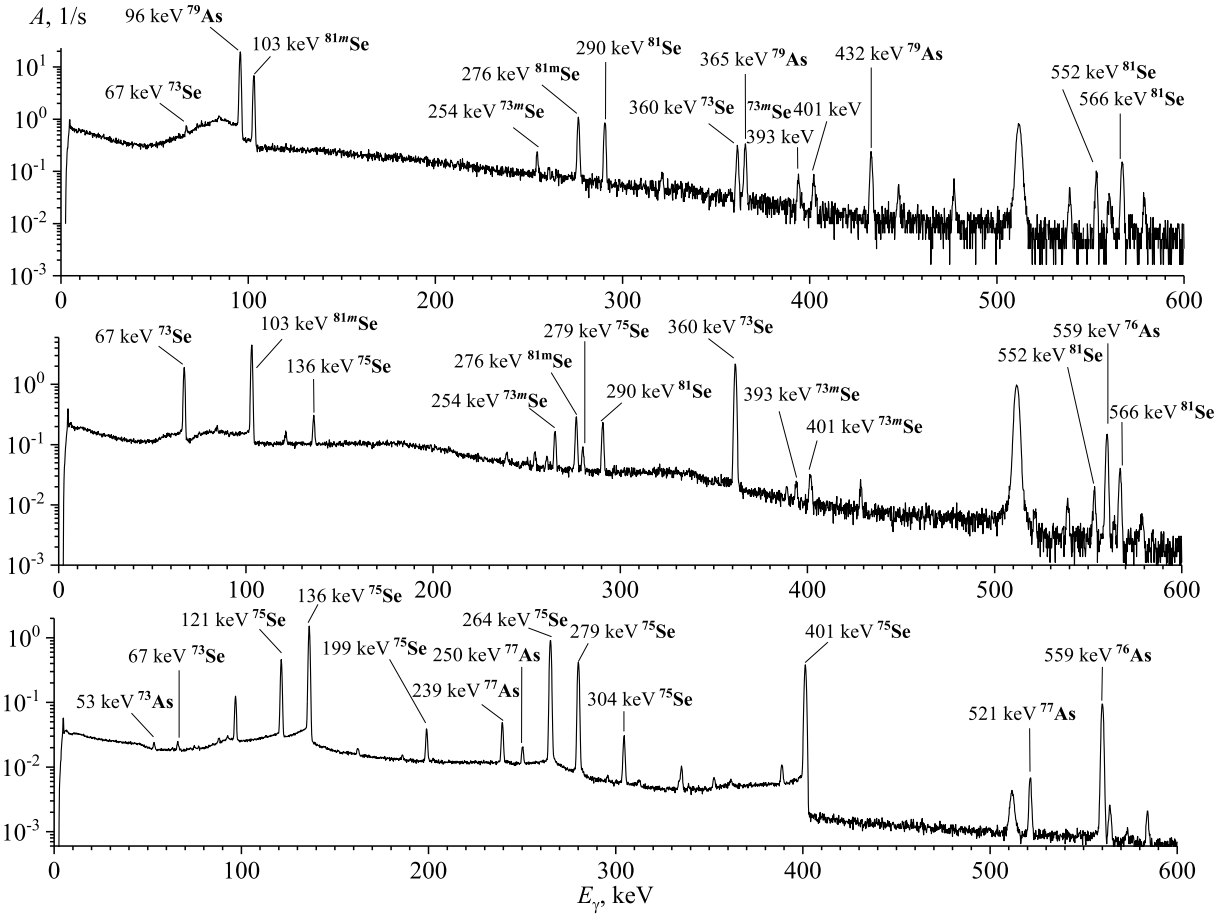

Fig. 1. Spectra of residual activity of the irradiated sample from a natural mixture of selenium isotopes (top-to-bottom) 10 min, 3 h, and 4 days after irradiation. The spectra measurement duration was 10 min, 1 h, and 1 day, respectively. The bremsstrahlung end-point energy used for the irradiation was 23 MeV.

Table 2. Spectroscopic data from Ref. [32] for the product nuclei from the photonuclear reactions on the stable isotopes of selenium.

Reaction product	Reactions	E_{th}/MeV	γ-ray energy, E_γ /keV (I_γ /%)	Half-life, $T_{1/2}$
^{73}Se	^{74}Se(γ,1n)	12.07	67.07 (70), 361.2 (97)	7.15 h
^{73m}Se	^{74}Se(γ,1n)	12.07	253.70 (2.36)	39.8 m
^{75}Se	^{76}Se(γ,1n)	11.15	121.12 (17.2), 136.00 (58.50), 264.66 (58.90), 279.54 (25.02), 400.66 (11.41)	119.78 d
^{81}Se	^{82}Se(γ,1n)	9.27	275.93 (0.68), 290.04 (0.56), 566.03 (0.224)	18.45 m
^{81m}Se	^{82}Se(γ,1n)	9.27	103.01 (12.8)	57.28 m
^{73}As	^{74}Se(γ,1p)	8.54	53.437 (10.6)	80.3 d
^{76}As	^{77}Se(γ,1p)	9.59	559.10 (45), 657.05 (6.2), 1216.08 (3.42)	1.09 d
^{77}As	^{78}Se(γ,1p)	10.39	239.01 (1.59), 249.81 (0.39), 520.65 (0.56)	1.62 d
^{79}As	^{80}Se(γ,1p)	11.41	95.73 (9.3), 365.0 (1.86), 432.1 (1.49)	9.01 m

Table 2. The nuclear data presented in columns 4−5 of Table 2 are taken from Ref. [32].

III. RESULTS AND DISCUSSION

The experimental yields of the reactions Y_{exp} were normalized to one electron of the accelerated beam incident on the bremsstrahlung target and calculated using the following formula:

$$Y_{exp} = \frac{S_p \cdot C_{abs}}{\epsilon \cdot I_\gamma} \frac{t_{real}}{t_{live}} \frac{1}{N} \frac{1}{N_e} \frac{e^{\lambda \cdot t_{cool}}}{(1-e^{-\lambda \cdot t_{real}})} \frac{\lambda \cdot t_{irr}}{(1-e^{-\lambda \cdot t_{irr}})}, \quad (1)$$

where S_p is the full-energy-peak area; ϵ is the full-en-

ergy-peak detector efficiency; I_γ is the gamma emission probability; $C_{\rm abs}$ is the correction for self-absorption of gamma rays in the sample; $t_{\rm real}$ and $t_{\rm live}$ are the real time and live time of the measurement, respectively; N is the number of atoms in the activation sample; N_e is the integral number of incident electrons; λ is the decay constant; $t_{\rm cool}$ is the cooling time; and $t_{\rm irr}$ is the irradiation time.

The yields $Y_{\rm theor}$ of photonuclear reactions representing the convolution of the photonuclear reactions cross section $\sigma(E)$ and the distribution density of the number of bremsstrahlung photons over energy per one electron of the accelerator $W(E, E_{\gamma\rm max})$ were determined as a result of the experiment. For the yield measurement of a natural mixture of isotopes, the result is the yield of isotope production in all possible reactions on the natural mixture:

$$Y_{\rm theor} = \sum_i \eta_i \int_{E_{\rm th}}^{E_{\gamma\rm max}} \sigma(E)\, W\left(E, E_{\gamma\rm max}\right) {\rm d}E, \tag{2}$$

where $E_{\gamma\rm max}$ is the kinetic energy of electrons hitting the tungsten radiator, E is the energy of bremsstrahlung photons produced on the radiator, $E_{\rm th}$ is the threshold of the studied photonuclear reaction, η is the percentage of the studied isotope in the natural mixture of selenium isotopes, and the index i corresponds to the number of the reaction contributing to the production of the studied isotope.

The total and partial cross sections σ(E) of the photonuclear reactions on the selenium isotopes were computed for the monochromatic photons using the TALYS1.96 code [22] with the standard parameters and CMPR [23]. The TALYS program analyzes all reactions occurring in the nucleus and transitions between states. Therefore, it is possible to determine not only the total cross sections of photonuclear reactions, but also the cross sections of reactions with the formation of specific states, in particular isomeric states. The CMPR calculates the cross sections of photonuclear reactions with production of a studied isotope, that is, the sum of the ground and isomeric states. The result of the yield measurement for a natural mixture of isotopes is the yield of isotope production in all possible reactions on the natural mixture. In our case, each radioactive nucleus was formed as a result of one specific photonuclear reaction, because the thresholds of other formation channels exceed 23 MeV.

The main disadvantage of bremsstrahlung beam experiments is that the yield of photonuclear reaction depends both on the studied cross section of the reaction $\sigma(E)$ and the shape of the bremsstrahlung spectrum $W(E, E_{\gamma\rm max})$, which is often known with insufficient accuracy. That is the reason why the data obtained from photonuclear experiments on bremsstrahlung beams are generally represented in terms of the relative yields or the integrated reaction cross section [33−35], flux weighted average cross section <σ> [36−43], or cross section per equivalent photon σ_q [35, 37, 43, 44].

The use of the relative yields makes it possible to obtain the dependence of the probability of photonuclear reactions on the maximum energy of bremsstrahlung under different experimental conditions. The calibration with respect to the yield of the most probable reaction excludes the influence of the total photon absorption cross section. In our case, the dominant reaction is ^{82}Se(γ,1n)$^{81m+g}$Se. Theoretical values of the relative yields can be calculated using the following formula:

$$Y_{{\rm rel},i} = \frac{\sum_i \eta_i \int_{E_{\rm th}}^{E_{\gamma\rm max}} \sigma_i(E)\, W\left(E, E_{\gamma\rm max}\right) {\rm d}E}{\eta_{\rm Se-82} \int_{E_{\rm th}}^{E_{\gamma\rm max}} \sigma_{(\gamma,n)}(E)\, W\left(E, E_{\gamma\rm max}\right) {\rm d}E}. \tag{3}$$

Owing to the assumption on the unchanged shape of the bremsstrahlung spectrum, the bremsstrahlung photon production cross section $\sigma(E, E_{\gamma\rm max})$ should be taken as the function $W(E, E_{\gamma\rm max})$:

$$Y_{{\rm rel},i} = \frac{\sum_i \eta_i \int_{E_{\rm th}}^{E_{\gamma\rm max}} \sigma_i(E)\sigma(E, E_m) {\rm d}E}{\eta_{\rm Se-82} \int_{E_{\rm th}}^{E_{\gamma\rm max}} \sigma_{(\gamma,n)}(E)\sigma(E, E_m) {\rm d}E}, \tag{4}$$

where $\sigma(E, E_{\gamma\rm max})$ is calculated based on the Zeltzer-Berger tables [45].

Figure 2 and Fig. 3 show experimental values of the relative yields of photoneutron reactions normalized to the yield of the reaction ^{82}Se(γ,1n)$^{81m+g}$Se (Table 3 contains exactly this). In the case of the photoneutron reactions, theoretical calculations and experimental results are in good agreement with each other. The experimental values of relative yields lie closer to the curves of TALYS and CMPR.

Figure 3 and Table 4 show the experimental values of the relative yields for the photoproton reactions on a natural mixture of selenium, in addition to the data computed with the use of the TALYS and CMPR codes. In the case of the ^{74}Se(γ,1p) reaction, theoretical calculations and experimental results are in good agreement with each other. In the case of relative yields for photoproton reactions on the heavy selenium isotopes, the theoretical values calculated using the CMPR are much larger than the TALYS results. For photoproton reactions on the isotopes of ^{77}Se, ^{78}Se, and ^{80}Se, the ratios of theoretical relative yields $Y_{\rm relCMPR}/Y_{\rm relTALYS}$ with increasing energy increase in the ranges of 2−5, 3−11, and 11−23, respectively. The experimentally obtained results lie closer to the

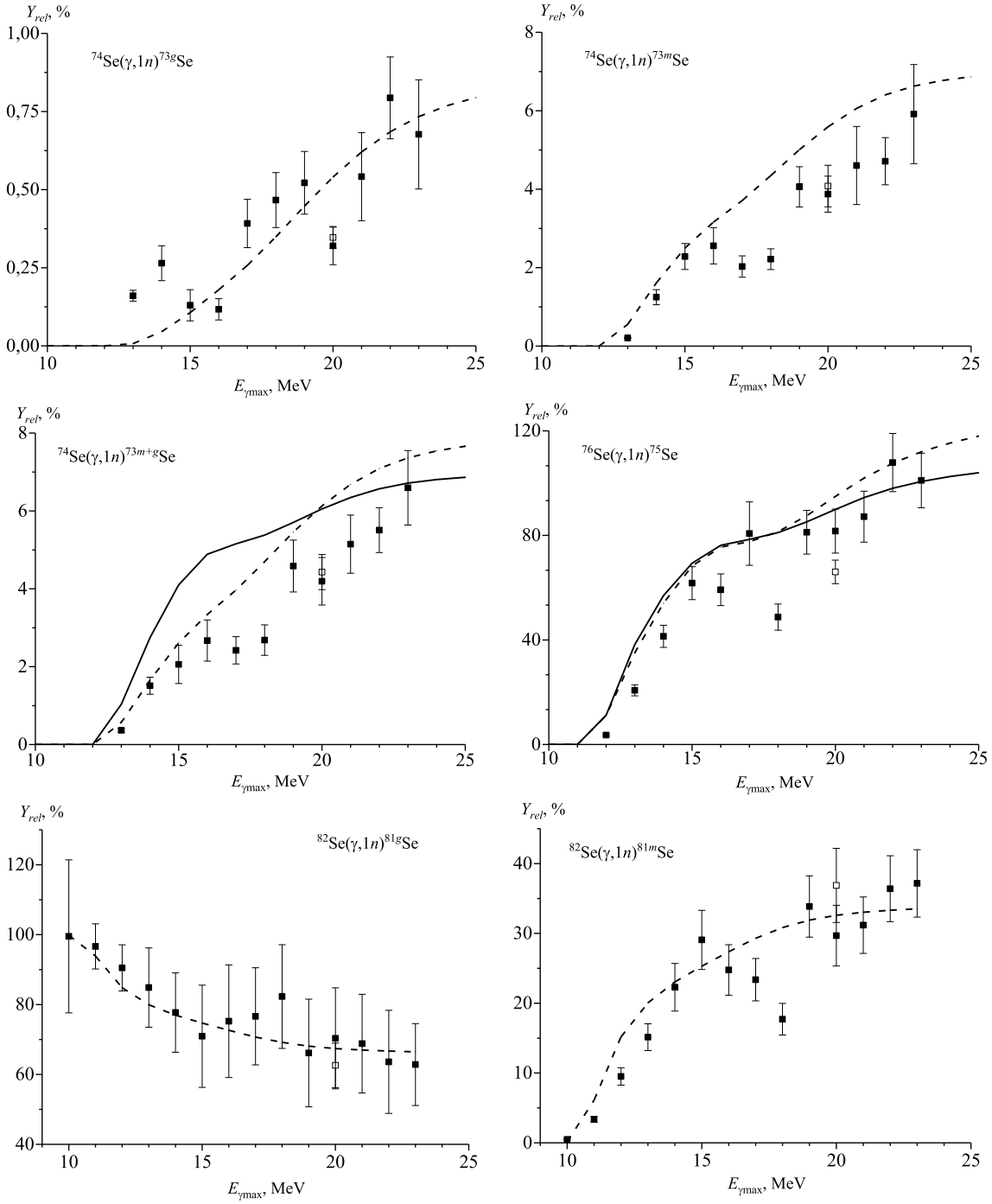

Fig. 2. Relative yields of ^{nat}Se(γ,1n) reactions as a function of bremsstrahlung end-point energy from the present work (solid rectangles), literature data [14] (open rectangles), and simulated values using the CMPR (solid lines) and TALYS code (dashed lines) based on monoenergetic photons.

theoretical curve according to the CMPR code. Including isospin splitting in the CMPR allows describing experimental data on reactions with proton escape in the energy range from 10 to 23 MeV. At the energy region above 25 MeV, in addition to isospin splitting, quadrupole resonance, the overtone of the giant resonance, and the quasideuteron mechanism make a significant contribution to the cross sections [14].

Unlike widely used numerical codes such as TALYS, GNASH, and EMPIRE, the CMPR considers not only the GDR and quasideuteron photoabsorption mechanism but also the contribution to the cross section of isovector quadrupole resonance and the GDR overtone in the calculation of the photoabsorption cross section. The energies

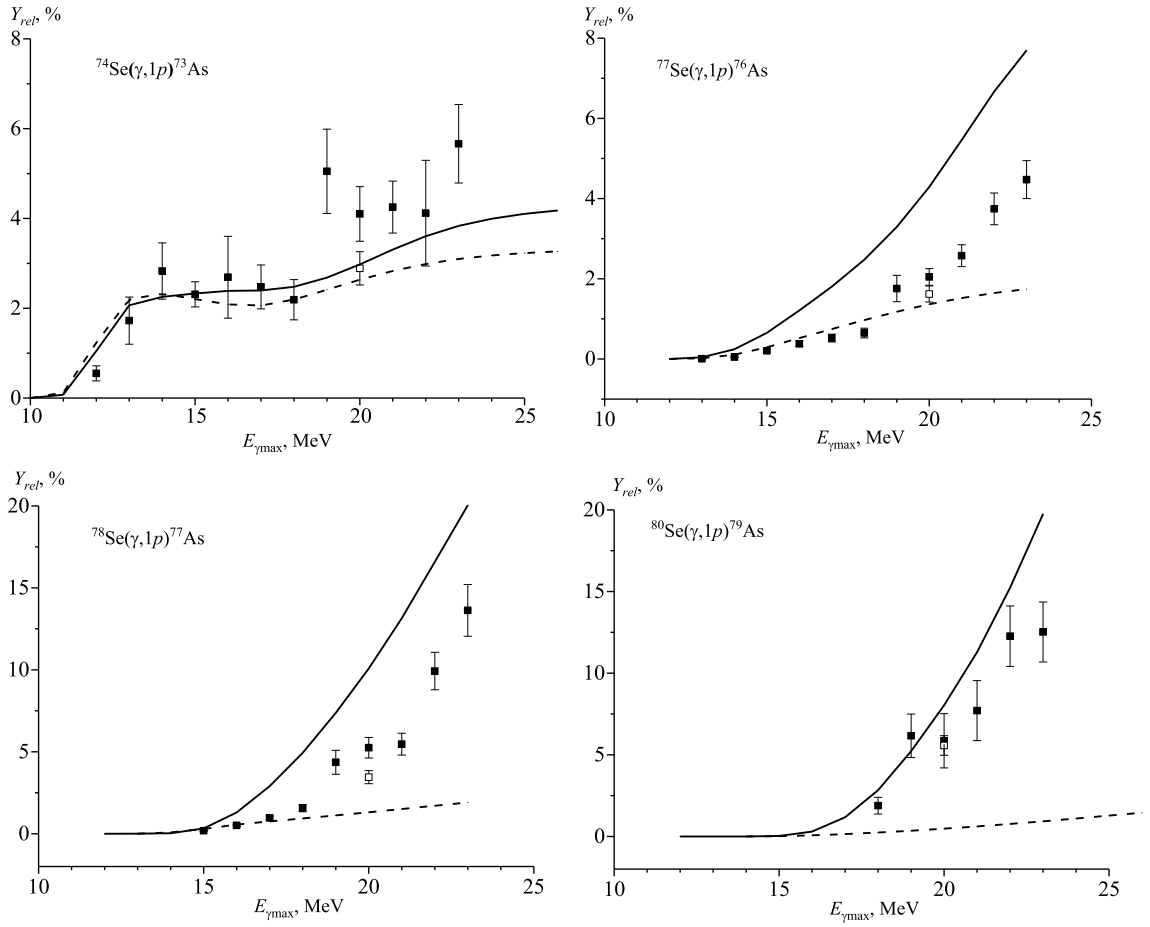

Fig. 3. Relative yields of ^{nat}Se(γ,1p) reactions as a function of bremsstrahlung end-point energy from the present work (solid rectangles), literature data [14] (open rectangles), and simulated values using the CMPR (solid line) and TALYS code (dashed line) based on monoenergetic photons.

and integral cross sections of this giant resonances are calculated in the framework of the semimicroscopic model with multipole–multipole residual forces [23].

In nuclei with $N \neq Z$, upon absorption of electric dipole γ photons, two branches of the GDR are excited, $T_<$ = T_0 and $T_>$ = T_0 + 1, where $T_0 = \frac{|N-Z|}{2}$. Figure 4 shows the excitations of the isospin components $T_<$ and $T_>$ of the GDR in initial nucleus (N, Z) and their decay according to the proton (N, $Z-1$) and neutron ($N-1$, Z) channels. From Fig. 4, it can be observed that the decay of excited GDR states with isospin $T_>$ = T_0 + 1 according to the neutron channel to low-lying states T = T_0 – 1/2 with neutron emission is forbidden, which leads to an increase in the reaction cross section (γ, 1p) and to a maximum shift of the reaction cross section (γ, 1p) with respect to reactions (γ, 1n) towards higher energies in the nucleus (N, Z).

The value of isospin splitting of the GDR is determined by the following relation (5):

$$\Delta E = E(T_>) - E(T_<) = \frac{60}{A}(T_0 + 1). \quad (5)$$

For isotopes ^{74,77,78,80}Se, the isospin increases from 3 to 6, which leads to an increase in the isospin splitting of the GDR for these isotopes from 3.24 to 5.25 MeV.

The ratio of the probabilities of excitation of states $T_>$ and $T_<$ is described by the following relation (6):

$$\frac{s(T_>)}{s(T_<)} = \frac{1}{T_0}\frac{1 - 1.5T_0A^{-2/3}}{1 + 1.5T_0A^{-2/3}}. \quad (6)$$

For isotopes ^{74,77,78,80}Se, the ratio $s(T_>)/s(T_<)$ decreases from 0.20 to 0.06 with an increase in the mass number A. Thus, for isotopes ^{74,77,78,80}Se, the isospin splitting of GDR increases with an increase in the mass number A, but the relative role of the excitation channel decreases.

The decay of excited GDR states with isospin $T_>$ = T_0 + 1 according to the neutron channel to low-lying states T = T_0 – 1/2 with neutron emission is forbidden, which leads to an increase in the reaction cross section (γ, 1p) and to a maximum shift of the reaction cross section (γ, 1p) with respect to reactions (γ, 1n) towards higher energies in the nucleus (N, Z). Figure 5 and Fig. 6 show the

Table 3. Relative yields of $^{nat}Se(\gamma,1n)$ reactions and comparison with theoretical results calculated on the basis of TALYS and CM-PR.

Reaction	$E_{\gamma max}$	Y_{rel}/%	$Y_{relTALYS}$/%	$Y_{relCMPR}$/%
$^{74}Se(\gamma, n)^{73g}Se$	13 MeV	0.16 ± 0.02	0.01	
	14 MeV	0.26 ± 0.06	0.04	
	15 MeV	0.13 ± 0.05	0.10	
	16 MeV	0.12 ± 0.03	0.17	
	17 MeV	0.39 ± 0.08	0.25	
	18 MeV	0.47 ± 0.09	0.33	
	19 MeV	0.52 ± 0.10	0.43	
	20 MeV	0.32 ± 0.06 0.35 ± 0.03 [14]	0.52	
	21 MeV	0.54 ± 0.14	0.59	
	22 MeV	0.79 ± 0.13	0.65	
	23 MeV	0.68 ± 0.17	0.70	
$^{74}Se(\gamma, n)^{73m}Se$	13 MeV	0.20 ± 0.01	0.53	
	14 MeV	1.25 ± 0.19	1.54	
	15 MeV	1.93 ± 0.33	2.39	
	16 MeV	2.56 ± 0.46	3.02	
	17 MeV	2.03 ± 0.27	3.55	
	18 MeV	2.22 ± 0.26	4.16	
	19 MeV	4.06 ± 0.51	4.79	
	20 MeV	3.87 ± 0.46 4.08 ± 0.53 [14]	5.35	
	21 MeV	4.60 ± 0.99	5.79	
	22 MeV	4.71 ± 0.60	6.12	
	23 MeV	5.92 ± 1.26	6.34	
$^{74}Se(\gamma, n)^{73m+g}Se$	13 MeV	0.37 ± 0.05	0.54	1.03
	14 MeV	1.51 ± 0.22	1.58	2.75
	15 MeV	2.06 ± 0.49	2.49	4.10
	16 MeV	2.67 ± 0.53	3.19	4.89
	17 MeV	2.42 ± 0.350	3.79	5.15
	18 MeV	2.68 ± 0.39	4.49	5.38
	19 MeV	4.58 ± 0.67	5.22	5.70
	20 MeV	4.19 ± 0.61 4.43 ± 0.45 [14]	5.86	6.05
	21 MeV	5.15 ± 0.75	6.39	6.35
	22 MeV	5.51 ± 0.58	6.78	6.57
	23 MeV	6.59 ± 0.96	7.04	6.71
$^{76}Se(\gamma, n)^{75}Se$	12 MeV	3.60 ± 0.37	10.78	11.20
	13 MeV	20.73 ± 2.12	34.22	38.23
	14 MeV	41.38 ± 4.24	52.70	56.98
	15 MeV	61.73 ± 6.32	66.58	69.35
	16 MeV	59.20 ± 6.06	73.65	76.19
	17 MeV	80.70 ± 12.13	75.65	78.46

Continued on next page

Table 3-continued from previous page

Reaction	$E_{\gamma max}$	Y_{rel}/%	$Y_{relTALYS}$/%	$Y_{relCMPR}$/%
	18 MeV	48.74 ± 5.01	79.38	81.07
	19 MeV	81.20 ± 8.36	85.38	85.19
	20 MeV	81.65 ± 8.42 66.05 ± 4.51 [14]	92.56	89.92
	21 MeV	87.18 ± 9.74	99.44	94.47
	22 MeV	107.88 ± 11.14	104.98	98.03
	23 MeV	101.02 ± 10.44	109.27	100.63
^{82}Se(γ, n)^{81g}Se	10 MeV	99.51 ± 21.89	99.84	
	11 MeV	96.64 ± 6.46	93.89	
	12 MeV	90.49 ± 6.59	84.83	
	13 MeV	84.86 ± 11.35	79.95	
	14 MeV	77.71 ± 11.36	76.95	
	15 MeV	70.93 ± 14.63	74.69	
	16 MeV	75.23 ± 16.11	72.63	
	17 MeV	76.63 ± 13.90	70.71	
	18 MeV	82.29 ± 14.84	69.17	
	19 MeV	66.14 ± 15.39	68.10	
	20 MeV	70.33 ± 14.45 62.59 ± 6.37 [14]	67.41	
	21 MeV	68.82 ± 14.12	66.97	
	22 MeV	63.60 ± 14.75	66.68	
	23 MeV	62.84 ± 11.72	66.48	
^{82}Se(γ, n)^{81m}Se	10 MeV	0.49 ± 0.08	0.16	
	11 MeV	3.36 ± 0.43	6.11	
	12 MeV	9.51 ± 1.24	15.17	
	13 MeV	15.13 ± 1.92	20.04	
	14 MeV	22.29 ± 3.41	23.04	
	15 MeV	29.07 ± 4.24	25.30	
	16 MeV	24.76 ± 3.61	27.36	
	17 MeV	23.37 ± 3.03	29.29	
	18 MeV	17.71 ± 2.26	30.82	
	19 MeV	33.86 ± 4.39	31.89	
	20 MeV	29.67 ± 4.35 36.87 ± 5.31 [14]	32.59	
	21 MeV	31.18 ± 4.04	33.03	
	22 MeV	36.39 ± 4.72	33.32	
	23 MeV	37.16 ± 4.82	33.52	

contribution of the $T_<$- and $T_>$-components to the theoretical cross sections and the relative yields for photoproton reactions of ^{74,77,78,80}Se isotopes. As can be observed in Fig. 5, in heavy isotopes of selenium, isospin splitting plays a significant role; by taking this into account, it is possible to correctly describe the GDR decay photoproton channel. The experimental data obtained by us also confirm this fact.

Among the nuclei heavier than ^{56}Fe, the formation of a group of 35 neutron-deficient stable nuclei starting with ^{74}Se, with very low abundance in the solar sistem, cannot be described by neutron capture reactions. Many production sites of the p-nuclei have been proposed: oxygen/neon layers of highly evolved massive stars dur-

Table 4. Relative yields of $^{nat}Se(\gamma,1p)$ reactions and comparison with theoretical results calculated on the basis of TALYS and CM-PR.

Reaction	$E_{\gamma max}$	Y_{rel}/%	$Y_{relTALYS}$/%	$Y_{relCMPR}$/%
$^{74}Se(\gamma, p)^{73}As$	12 MeV	0.55 ± 0.17	1.23	1.05
	13 MeV	1.72 ± 0.52	2.20	2.06
	14 MeV	2.83 ± 0.63	2.32	2.25
	15 MeV	2.31 ± 0.28	2.20	2.33
	16 MeV	2.69 ± 0.91	2.08	2.39
	17 MeV	2.47 ± 0.49	2.06	2.39
	18 MeV	2.19 ± 0.45	2.19	2.48
	19 MeV	5.05 ± 0.94	2.41	2.68
	20 MeV	4.10 ± 0.61 2.89 ± 0.37 [14]	2.64	2.97
	21 MeV	4.25 ± 0.58	2.83	3.30
	22 MeV	4.12 ± 1.18	2.98	3.60
	23 MeV	5.66 ± 0.87	3.09	3.83
$^{77}Se(\gamma, p)^{76}As$	13 MeV	0.005 ± 0.001	0.0004	0.002
	14 MeV	0.05 ± 0.01	0.02	0.04
	15 MeV	0.21 ± 0.04	0.11	0.24
	16 MeV	0.38 ± 0.07	0.29	0.65
	17 MeV	0.52 ± 0.09	0.52	1.21
	18 MeV	0.65 ± 0.12	0.75	1.81
	19 MeV	1.76 ± 0.33	0.97	2.47
	20 MeV	2.05 ± 0.21 1.62 ± 0.20 [14]	1.18	3.29
	21 MeV	2.57 ± 0.27	1.36	4.29
	22 MeV	3.74 ± 0.39	1.52	5.46
	23 MeV	4.47 ± 0.47	1.65	6.67
$^{78}Se(\gamma, p)^{77}As$	15 MeV	0.18 ± 0.03	0.29	0.32
	16 MeV	0.51 ± 0.07	0.56	1.29
	17 MeV	0.96 ± 0.13	0.76	2.90
	18 MeV	1.56 ± 0.22	0.93	4.94
	19 MeV	4.36 ± 0.73	1.12	7.37
	20 MeV	5.24 ± 0.63 3.45 ± 0.40 [14]	1.31	10.08
	21 MeV	5.46 ± 0.66	1.51	13.14
	22 MeV	9.92 ± 1.14	1.71	16.59
	23 MeV	13.63 ± 1.57	1.91	20.04
$^{80}Se(\gamma, p)^{79}As$	18 MeV	1.89 ± 0.51	0.24	2.83
	19 MeV	6.16 ± 1.33	0.35	5.22
	20 MeV	5.86 ± 1.66 5.57 ± 0.60 [14]	0.48	8.03
	21 MeV	7.71 ± 1.84	0.61	11.29
	22 MeV	12.27 ± 1.85	0.77	15.23
	23 MeV	12.52 ± 1.84	0.93	19.75

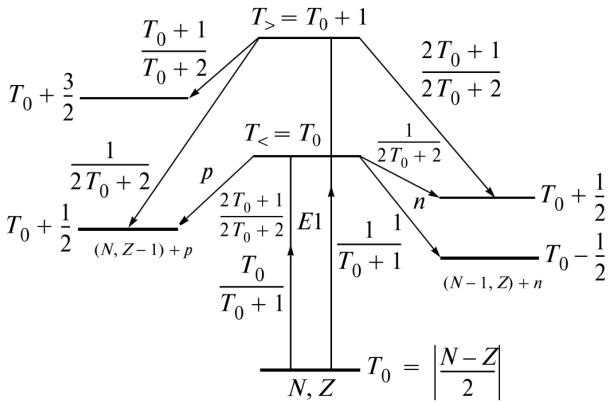

Fig. 4. Scheme of excitation of states $T_<$ and $T_>$ in the nucleus (N, Z) and their decay along the proton channel (N, $Z-1$) and neutron channel ($N-1$, Z).

ing their presupernova phase [46] and during their supernova explosion [47], X-ray novae [48], neutrinodriven winds originating from a nascent neutron star shortly after supernova explosion [49], Type Ia supernova explosions [50], and helium-accreting CO white dwarfs of sub-Chandrasekhar mass [51]. Among them, the most promising is the oxygen/neon layers during a Type II supernova explosion. The p-nuclei are synthesized by the photodisintegration of s-nuclei (s-process seeds) produced in the layers during the core helium burning in the progenitor. The production of p-nuclei via the subsequent photodisintegration is referred to as a p-process [52]. Photonuclear reactions represent a threshold; therefore, a necessary condition for their occurrence is a high temperature $T = 1 - 3.5$ K [47], which is fulfilled when a shock wave passes through the layers of a pre-supernova star of the SnII type after the collapse of the supernova core [53−54]. For the synthesis of p-nuclei, in addition to the considered gamma-ray processes on equilibrium photons, other models have been proposed, such as nuclear reactions of proton capture (p, γ), (p, n), reactions under the influence of powerful fluxes of neutrino radiation from the stellar core, and reactions of rapid capture of protons accreted on the surface of a neutron star . To describe the formation and decay of p-nuclei as a result of photonuclear reactions, it is necessary to accurately know the yields of photoproton and photoneutron reactions, the correct calculation of which is impossible without taking into account the isospin splitting of the GDR. The p-pro-

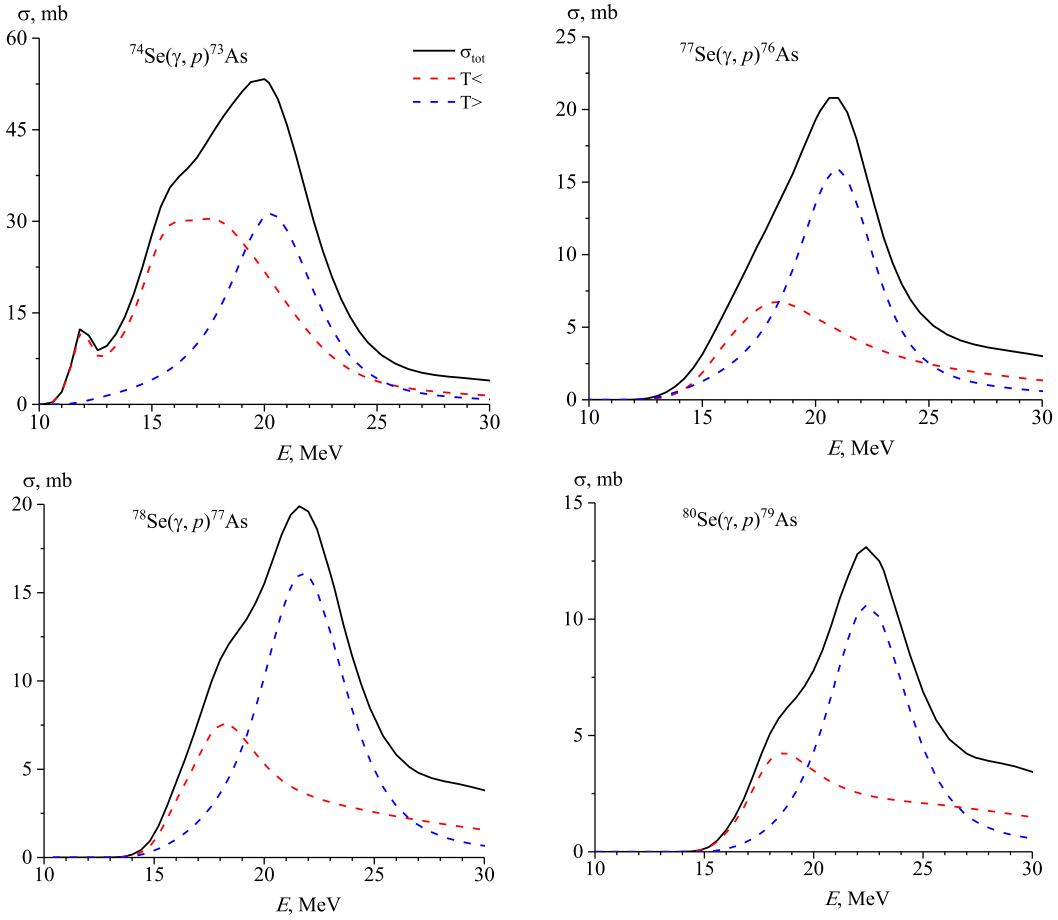

Fig. 5. (color online) Cross section reactions and cross sections of the GDR components $T_< = T_0$ and $T_> = T_0 + 1$ for reaction (γ, 1p) on ^{74,77,78,80}Se isotopes.

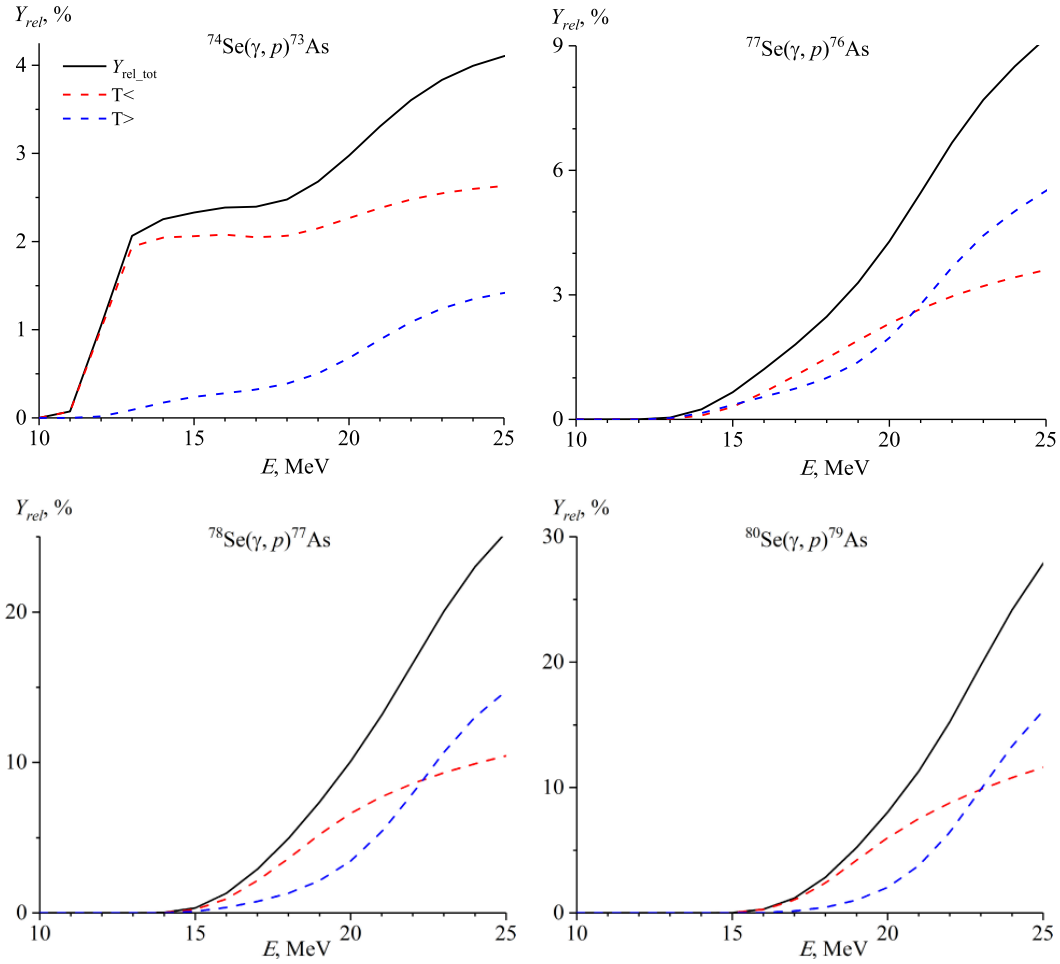

Fig. 6. (color online) Contribution of the $T_<$ and $T_>$ components to the theoretical relative yields for photoproton reactions on a natural mixture of selenium isotopes.

cess involves positron production and capture, proton capture, and (γ, n) or (p, n) reactions starting from the s- and r-isotopes as seed nuclei. Figure 7 shows the paths of the formation and decay of ^{74}Se p-nuclide in stellar nucleosynthesis. Figure 8(a) shows the cross sections of (γ, 1n), (γ, 2n), and (γ, 3n) reactions corresponding to the isotopes ^{75}Se, ^{76}Se, and ^{77}Se calculated based on the CMPR. According to the data shown in Fig. 8 (a), the main reactions of the formation of the isotope ^{74}Se are (γ, 1n) and (γ, 2n). This leads to a significant buildup of the p-nucleus, assisted by a moderately strong ^{75}As(γ, n)^{74}As(β^-)^{74}Se branch.

As shown in Fig 7, there are three competing pathways for the decay of ^{74}Se: (γ, 1n) (12.07 MeV), (γ, 1p) (8.54 MeV), and (γ, α) (4.07 MeV). ^{74}Se has a two-neutron separation energy (20.46 MeV) greater than 20 MeV, and thus, it cannot be destroyed via the (γ, 2n) reaction. To compare the main destruction channels of the bypassed nucleus, the cross sections of (γ, n), (γ, p), and (γ, α) reactions on the isotope ^{74}Se calculated based on TALYS are shown in Fig. 8 (b). The calculated reaction cross sections at maximum GDR are 100, 35, and 3 mb, respectively. The results of our research will allow us to experimentally compare the ^{74}Se(γ, 1n) and ^{74}Se(γ, 1p) reactions. Figure 8 (c) shows the relative yields of the ^{74}Se(γ, 1n) and ^{74}Se(γ, 1p) reactions. As can be observed from Fig. 8 (c), the two main competing ways of decay of ^{74}Se are almost equal. The reaction product ^{74}Se(γ, α)^{70}Ge is stable and it is impossible to estimate the probability of passing this reaction using the gamma activation method.

IV. CONCLUSION

The present study addressed the measurements of relative yields for the photonuclear reactions on a natural mixture of selenium using bremsstrahlung end-point energies of 10 to 23 MeV. The bremsstrahlung photon flux was computed in the Geant4.11.1 code. The experimental results were compared with calculations using the TALYS model with the standard parameters and the CMPR. For the obtained photoneutron reactions, a good agreement was observed between the experimental relative yields and calculations according to the TALYS program

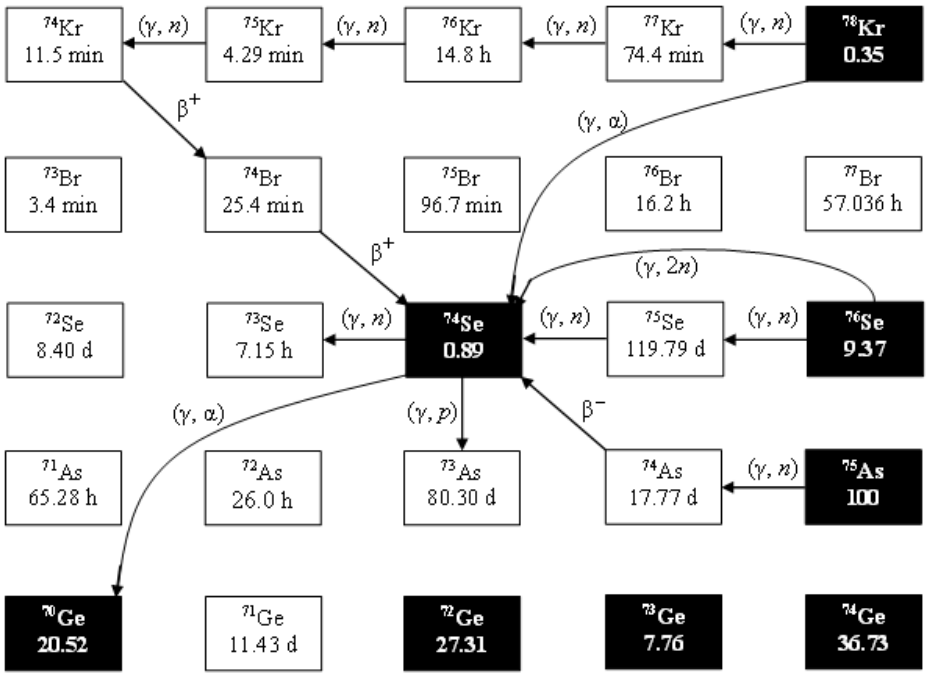

Fig. 7. Paths of the production and decay of ^{74}Se *p*-nuclide in stellar nucleosynthesis.

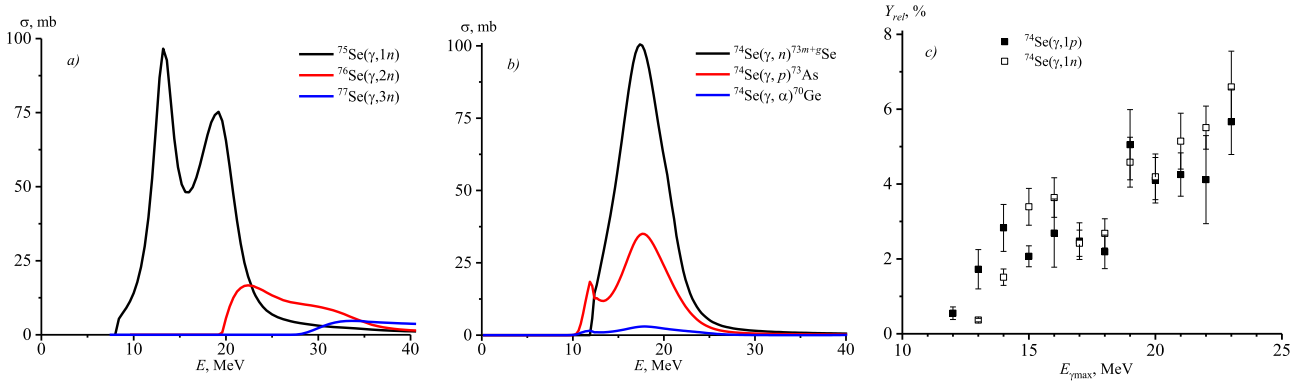

Fig. 8. (color online) (a) Cross sections of the (γ, 1*n*), (γ, 2*n*), and (γ, 3*n*) reactions corresponding to the isotopes ^{75}Se, ^{76}Se, and ^{77}Se calculated based on TALYS. (b) Cross sections of the (γ, *n*), (γ, *p*), and (γ, α) reactions on the isotope ^{74}Se calculated based on TALYS. (c) Relative yields of reactions with the emission of a neutron (open rectangles) and a proton (solid rectangles) as a function of bremsstrahlung end-point energy.

and CMPR framework. For the photoproton reaction on the light isotope ^{74}Se, there was no difference between the data calculated using TALYS and CMPR and the experimental values. On the heavy selenium isotopes, the theoretical relative yields calculated using the CMPR were much larger than the TALYS results. Including isospin splitting in the CMPR allows describing experimental data on reactions with proton escape in the energy range from 10 to 23 MeV. Therefore, taking into account isospin splitting is necessary for a correct description of the decay of the GDR. At the energy region above 25 MeV, in addition to isospin splitting, quadrupole resonance, the overtone of the giant resonance, and the quasideuteron mechanism make a significant contribution to the cross sections. The study of photonuclear reactions on selenium isotopes is important for understanding the formation and decay of bypassed nuclei during nucleosynthesis.

ACKNOWLEDGMENT

The authors would like to thank the staff of the MT-25 microtron of the Flerov Laboratory of Nuclear Reactions, Joint Institute for Nuclear Research, for their cooperation in the realization of the experiments.

References

[1] A. Zilges, D. L. Balabanski, J. Isaak *et al*., Prog. Part. Nucl. Phys. **122**, 103903 (2022)
[2] N. Pietralla, AIP Conf. Proc. 1462 195 (2012)
[3] C. H. Lin, J. M. Wu, T. C. Chiu *et al*., Appl. Radiat. Isot. **70**, 1564 (2012).
[4] D. J. S. Findlay, Nucl. Instrum. Methods B **50**, 314 (1990)
[5] A. M. Goryachev and G. N. Zalesnyy, Voprosy Teoreticheskoy i Yadernoy Fiziki, 8, 121 (1982)
[6] V. M. Mazur, I. V. Sokolyuk, Z. M. Bigan, J Phys Atomic Nuclei, 54, 541(1991)
[7] T. D. Thiep, T. T. An, N. T. Khai *et al*., JRN **292**, 1035 (2012)
[8] S. R. Palvanov and O. Razhabov, J. Atomic Energy **87**, 75 (1999)
[9] A. D. Antonov, N. P. Balabanov, A. G. Belov *et al*., MINSK, 286 (1991)
[10] M. G. Davydov, V. G. Magera, A. V. Trukhov *et al*., At. Energy **58**, 56 (1985)
[11] Yu. P. Gangrskiy, P. Zuzaan, N. N. Kolesnikov *et al*., J. IZV **65**, 111 (2001)
[12] F. Z. Hien, N. K. Zui, and N. T. An, SNP **35**, 145 (1982)
[13] F. A. Rasulova, R. A. Aliev, S. S. Belyshev *et al*., Phys. At. Nucl., 86, 5 (2023) in print
[14] F. A. Rasulova, R. A. Aliev, S. S. Belyshev *et al*., NIM A **1054**, 168428 (2023).
[15] P. Carlos, H. Beil, R. Bergere *et al*., Nucl. Phys. A **258**, 365 (1976).
[16] S. A. Yates, B. Fallin, C. R. Howell *et al*., Phys. Rev. C **98**, 054621 (2018)
[17] F. Kitatani, H. Harada, S. Goko *et al*., NST **48**, 1017 (2011)
[18] F. Kitatani, H. Harada, S. Goko *et al*., NST **53**, 475 (2016)
[19] F. Kitatani, H. Harada, S. Goko *et al*., NST **47**, 367 (2010)
[20] A. Makinaga, H. Utsunomiya, S. Goriely *et al*., Phys. Rev. C **79**, 025801 (2010)
[21] M. Arnould and S. Goriely, Phys. Rep. **38**, 1 (2003)
[22] A. Koning, S. Hilaire, and S. Goriely, User Manual, 2021 https://www-nds.iaea.org/talys/tutorials/talys_v1.96.pdf
[23] B. S. Ishkhanov and V. N. Orlin, Phys. At. Nucl. **78**, 557 (2015)
[24] A. Juarez, I. A. Vega, L. S. Mayorga *et al*., Sci. Total Environ. **815**, 152760 (2022)
[25] M. Jennewein, M. A. Lewis, D. Zhao *et al*., Clin. Cancer Res. **14**, 1377 (2008)
[26] V. A. Sanders and C. S. Cutler, Nucl. Med. Biol. **92**, 184 (2021)
[27] O. D. Maslov and S. N. Dmitriev, *Use of MT-25 microtron for scientific and applied investigations* https://inis.iaea.org/collection/NCLCollectionStore/_Public/35/022/35022466.pdf
[28] S. S. Belyshev, A. N. Ermakov, B. S. Ishkhanov *et al*., Nucl. Instrum. Methods Phys. Res. A **745**, 133 (2014)
[29] B. S. Ishkhanov and A. A. Kuznetsov, Moscow Univ. Phys. Bull. **68**, 279 (2013)
[30] S. S. Belyshev, K. A. Stopani, S. Yu. Troschiev *et al*., Moscow Univ. Phys. Bull. **66**, 363 (2011)
[31] J. Frana, J. Radioanal. Nucl. Chem. **257**, 583 (2003)
[32] Nudat 2.8, National Nuclear Data Center, Brookhaven National Laboratory http://www.nndc.bnl.gov/nudat2/
[33] B. S. Ishkhanov, V. N. Orlin, and S. Yu. Troschiev, Phys. At. Nucl. **75**, 253 (2012)
[34] K. A. Stopani, Cand. Sci. (Phys. Math.) Dissertation (Moscow, 2012) http://www.sinp.msu.ru/en/preprint/8290
[35] S. S. Belyshev, B. S. Ishkhanov, A. A. Kuznetsov *et al*., Moscow Univ. Phys. Bull. **75**, 513 (2020)
[36] A. N. Vodin, O. S. Deiev, V. Yu. Korda *et al*., Nucl. Phys. A **1014**, 122248 (2021)
[37] A. N. Vodin, O. S. Deiev, I. S. Timchenko *et al*., Eur. Phys. J. A **57**, 207 (2021)
[38] A. N. Vodin, O. S. Deiev, I. S. Timchenko *et al*., Eur. Phys. J. A **57**, 208 (2021)
[39] H. Naik, G. N. Kim, R. Schwengner *et al*., Nucl. Phys. A **916**, 168 (2013)
[40] H. Naik, G. N. Kim, R. Schwengner *et al*., Eur. Phys. J. A **56**, 264 (2019)
[41] P. D. Remizov, M. V. Zheltonozhskaya, A. P. Chernyaev *et al*., Eur. Phys. J. A **59**, 141 (2023)
[42] P. D. Remizov, M. V. Zheltonozhskaya, A. P. Chernyaev *et al*., Phys. Atom. Nucl. **85**, 818 (2023)
[43] V. Di Napoli, A. M. Lacerenza, F. Salvetti *et al*., Lett. Nuovo Cimento **1**, 835 (1971)
[44] O. S. Deiev, I. S. Timchenko, S. N. Olejnik *et al*., Chin. Phys. C **6**, 064002 (2022)
[45] M. J. Berger and S. M. Seltzer, Phys. Rev. C **2**, 621 (1970)
[46] M. Arnould, Astron. Astrophys. 46, 117 (1976)
[47] S. E. Woosley and W. M. Howard, Astrophysical Journal Supplement Series 36, 285 (1978)
[48] H. Schatz, A. Aprahamian, J. Gorres *et al*., Phys. Rep. **294**, 167 (1998)
[49] R. D. Hoffman, S. E. Woosley, G. M. Fuller *et al*., Astrophys. J. **460**, 478 (1996)
[50] W. M. Howard, B. S. Meyer, and S. E. Woosley, Astrophys. J. Lett. **373**, L5 (1991)
[51] S. Goriely, J. Jose, M. Hernanz *et al*., Astron. Astrophys. **383**, L27 (2002)
[52] S. Fujimoto, M. Hashimoto, O. Koike *et al*., The Astrophys. J. **585**, 418 (2003)
[53] C. Travaglio, F. K. Röpke, R. Gallino *et al*., Astrophys. J. **739**, 93 (2011)
[54] M. Rayet, N. Prantzos, and M. Arnould, Astron. Astrophys. 227, 271 (1990)